Real-space Observation of a Transition Metal Complex Dissociation and Energy Redistribution

Aviad Schori[1], Elisa Biasin[1,2], Ambar Banerjee[3,4], Sébastien Boutet[5], Philip H. Bucksbaum[1,6], Sergio Carbajo[5], Kelly J. Gaffney[1,7], James Glownia[5], Robert Hartsock[1], Kathryn Ledbetter[1], Andreas Kaldun[1], Jason E. Koglin[5], Kristjan Kunnus[1], Thomas J. Lane[5], Mengning Liang[5], Michael P. Minitti[5], Jordan T. O'Neal[1], Robert M. Parrish[1], Frederic Poitevin[1], Jennifer M. Ruddock[8], Silke Nelson[5], Brian Stankus[8,9], Peter M. Weber[8], Thomas J.A. Wolf[1], Michael Odelius[3], Adi Natan[1*]

[1*]Stanford PULSE Institute, SLAC National Accelerator Laboratory, 2575 Sand Hill Rd, Menlo Park, 94025, CA, USA.

[2]Physical Sciences Division, Pacific Northwest National Laboratory, 902 Battelle Blvd, Richland, 99352 , WA, USA.

[3]Department of Physics, Stockholm University, AlbaNova University Center, Stockholm, SE-106 91 , Sweden.

[4]Research Institute for Sustainable Energy (RISE), TCG Centres for Research and Education in Science and Technology, Kolkata, 700091, India.

[5]Linac Coherent Light Source, SLAC National Accelerator Laboratory, 2575 Sand Hill Rd, Menlo Park, 94025, CA, USA.

[6]Department of Physics and Applied Physics, Stanford University, 382 Via Pueblo Mall, Stanford, 94305, CA, USA.

[7]Department of Chemistry, Stanford University, 33 Campus Drive, Stanford, 94305, CA, USA.

[8]Department of Chemistry, Brown University, Providence, 02912, RI, USA.

[9] Department of Chemistry and Biochemistry, Western Connecticut State University, Danbury, 06810, CT, USA.

*Corresponding author(s). E-mail(s): natan@stanford.edu;

Abstract

Mechanistic insights into photodissociation dynamics of transition metal carbonyls, like $Fe(CO)_5$, are fundamental for understanding active catalytic intermediates. Although extensively studied, the ultrafast structural dynamics of these systems remain elusive. Using ultrafast X-ray scattering, we uncover the ultrafast photochemistry of $Fe(CO)_5$ in real space and time, observing synchronous oscillations in atomic pair distances, followed by a prompt rotating CO release preferentially in the axial direction. This behavior aligns with simulations, reflecting the interplay between the axial Fe-C distances' potential energy landscape and non-adiabatic transitions between metal-to-ligand charge-transfer states. Additionally, we characterize a secondary delayed CO release associated with a reduction of Fe-C steady state distances and structural dynamics of the formed $Fe(CO)_4$. Our results quantify energy redistribution across vibration, rotation, and translation degrees of freedom, offering an ultrafast microscopic view of complex structural dynamics, enhancing our grasp on $Fe(CO)_5$ photodissociation and advancing our understanding of transition metal catalytic systems.

1 Introduction

The use of light to drive synthesis has seen tremendous growth in the last decade [1, 2]. In particular, organometallic photocatalysts such as transition metal carbonyls [3–5], are pivotal for understanding the mechanisms of metal-ligand bond breakage upon light exposure, a cornerstone issue in chemistry with implications521 in synthesis and catalysis. The efficiency and selectivity of photocatalytic processes are directly related to the molecular-level mechanisms of energy flow and transformation, including internal vibrational relaxation, rotational motions, and dissociation events in these systems [6, 7]. By understanding these ultrafast structural dynamics, chemists can design more effective catalytic systems and optimize reaction conditions for practical applications.

Extensive research on iron pentacarbonyl $Fe(CO)_5$, particularly on processes triggered by metal-to-ligand charge-transfer (MLCT), has used various methods to explore its photochemistry revealing the dissociation of carbon monoxide (CO) from $Fe(CO)_5$ into $Fe(CO)_4$ and then $Fe(CO)_3$ in gas phase dynamics [8–14]. The initial experimental studies used 266 nm UV pulses to photoexcite $Fe(CO)_5$ in the gas phase and probed its dynamics using optical ionization [9–11] measuring various time constants up to the few ps range, without assigning the different possible species. However, a sequential singlet pathway was suggested, with the assumption that intersystem crossings are not viable in such timescales. The suggested pathway was prompt dissociation from excited singlet-state $Fe(CO)_5$ to the lowest energy singlet state of $Fe(CO)_4$ ($^1A_1$), following which, a second CO dissociation to $Fe(CO)_3$ with a time constant of 3 ps. Time-resolved electron diffraction experiments [15] validated the singlet-state $Fe(CO)_4$

using two-photon absorption at 620 nm and a temporal resolution of 10–20 ps. Direct evidence of the singlet and sequential aspect of the dissociation of multiple CO ligands has been established with a temporal resolution of 1 ps [12] using time-resolved valence and core-level photoelectron XUV spectroscopy.

Recently, a theoretical study suggested that the MLCT transition causes Fe-C bond oscillations in the trigonal bipyramidal complex [16]. As a result, the first CO dissociation process involves a probabilistic sequential dissociation, that occurs each time non-adiabatic transitions happen between manifolds of bound MLCT and dissociative metal-centered (MC) excited states (Figure 1).

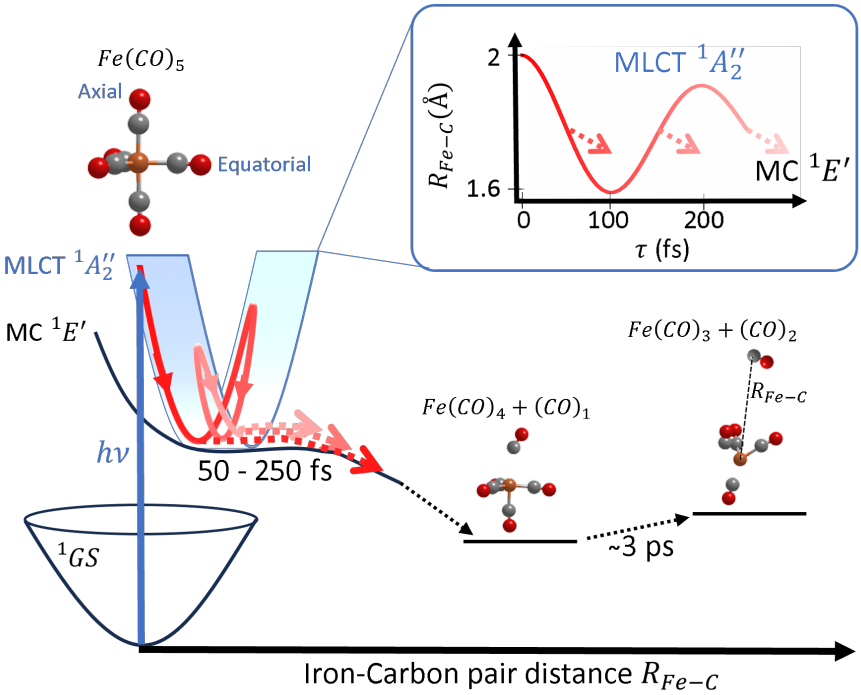

Fig. 1 Schematic depicting $Fe(CO)_5$ photochemistry: UV (266 nm) pulse excites $Fe(CO)_5$ from its ground state (GS) to a metal-to-ligand charge-transfer excited state (MLCT). This transition leads to periodic crossovers to the dissociative metal-centered (MC) state, observed through a symmetric stretch mode in axial Fe-C bonds. Each MLCT to MC crossover may induce dissociation of the first CO ligand (inset, dashed arrows represent crossover), occurring approximately every 100 fs, generating hot $Fe(CO)_4$ and a rotating dissociating CO. Subsequently, a second CO is dissociating at a slower timescale ($\sim$ 3 ps).

While studies probed the population transfer between electronic states, to fully understand how photon energy transforms into both electronic and nuclear dynamics, it's crucial to observe ultrafast structural dynamics, which requires probing atomic motions on the scale of angstroms and femtoseconds. Such direct observation is key to understanding the creation of specific reactive intermediates, and despite its importance, achieving this level of detail has so far proved difficult.

Ultrafast x-ray scattering (UXS) and MeV ultrafast electron diffraction (UED) studies have become viable tools to uncover ultrafast structural dynamics of increasing complexity, from wavepacket vibration and dissociation of diatomic molecules to chemical reactions and structural changes of molecules in solution environments [17–31]. Electron diffraction offers a greater momentum transfer range (Q$\sim$12Å^{-1}) that allows in principle the direct inversion to real space of the scattering signal, but often at lower temporal resolution. Ultrafast X-ray pulses from free electron lasers (FELs) often access better temporal resolution but with a restricted range (Q$\sim$4Å^{-1}) that has limited the inversion and interpretation of the scattering signals and required complementary support through modeling and simulations [32–34]. Recent improvements in inversion methods that account for limitations originating from the measurement, including a restricted Q range [35], enable the robust real-space inversion central to this study.

Here, we demonstrate the use of UXS and real-space inversion to directly observe the photochemistry of $Fe(CO)_5$ with atomic resolution in space and time. We observe its initial coherent motion, prompt dissociation that includes molecular rotation, and the rovibration dynamics of the intermediate $Fe(CO)_4$. We also observe and quantify the secondary dissociation to $Fe(CO)_3$. We resolve multiple simultaneous atomic motions on femtosecond timescales of a first-row transition metal complex in the gas phase, where charge density distance distributions from different atom pairs contribute similarly to the signal (Figure 2a), making it the first observation, to our knowledge, of ultrafast gas phase scattering from a transition metal complex. We observe microscopic real-space details of coherent to thermal pair density dynamics, which is an intuitive and independent probe for processes that take place across timescales, despite the restricted momentum transfer range measured (Figure 2b). The time-resolved real-space information is recovered in a model-free way, which enables a straightforward comparison with ab initio simulations, offering a path for robust validation of theory for the challenging case of transition-metal excited-state dynamics.

2 Results and Discussion

For non-periodic samples such as in gas or the solution phase, assuming the independent atom model, the scattering information of typical experiments only encodes the distances between each pair of charges captured by the pair density function. In Figure 2a, we show how the early excited state dynamics of $Fe(CO)_5$ is captured by atomic pair charge density difference $\Delta PD(R,\tau)=PD(R,\tau)_{on}-PD(R)_{off}$, subtracting the optical pump laser-on signal at delay time τ after photoexcitation from the laser-off reference signal, using a simulation based on semi-classical excited state molecular dynamics, that is limited to the first CO loss dynamics (Supplementary Discussions 2). Positive intensities indicate new distances with a magnitude corresponding to the charge product of the contributing atom pairs, and negative peaks indicate the drop in steady-state pair distances. As a result, even though the motion originates in the Fe-C bond distances (region α), a change in Fe-C pair distances affects many other atom pair distances that act as "spectators", as seen during the first 200 fs (region β). This is because atoms of type X that remain stationary to the Fe-C motion, will

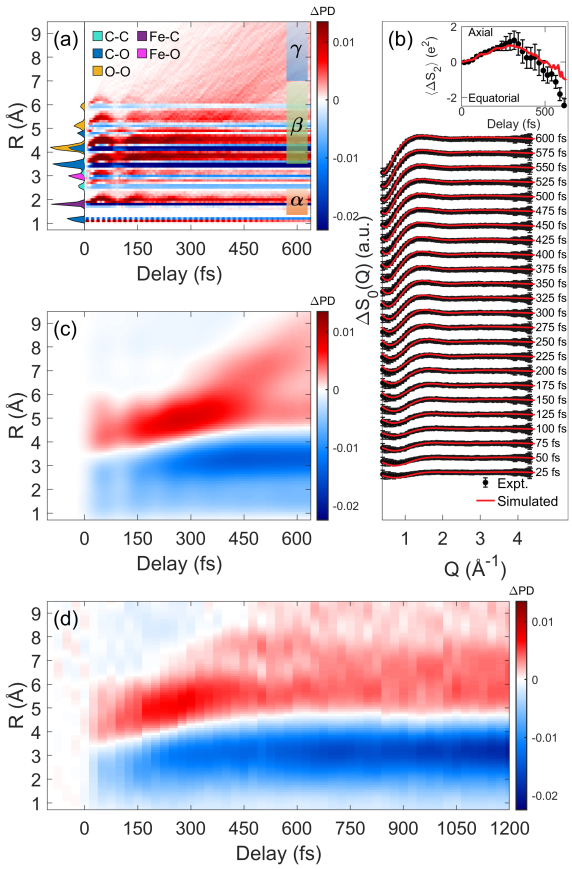

Fig. 2 (a) The simulated pair density difference ΔPD for photoexcited $Fe(CO)_5$ obtained from averaging 85 trajectories (Supplementary Discussion 2), and derived by subtracting the steady state pair density (perpendicular area plot, colors encode atom pair types) from the time-dependent density. The motion initiates within the Fe-C bond (α region), however, it is also observed across most pairs due to the spectator effect (see text). (b) Simulated and experimental isotropic scattering difference signal ΔS_0 for photoexcited $Fe(CO)_5$ in momentum-transfer space for a series of time delays. (inset) The averaged anisotropy of the scattering signals $\langle \Delta S_2 \rangle$ for Q<0.9Å^{-1} shows that axial CO is more likely to be first lost (Supplementary Discussion 3). (c) The inversion of the simulated scattering captures PD oscillations at β region (4−7Å), following dissociation seen as a density increase at 200−400 fs, coinciding with the anisotropy dynamics. At longer delays, the dissociating PD separates from the parent molecule observed at γ region (R>7Å) , where the PD modulation at ∼7.5Å is assigned to a CO rotation motion. (d) The real-space inverted experimental scattering signal captures similar early dynamics, as well as a second CO loss at delays >700 fs, manifested by a further decrease (increase) of density at the α (γ) range.

contribute to correlated Fe-X and C-X motions, effectively amplifying the original Fe-C motion. We also note that the contribution to ΔPD is distributed across several types of atomic pairs that can also overlap. For example, the dominant ΔPD is found around 4 Å as a result of multiple C-O and O-O pairs that are spectators to the early dynamics. Early on, the CO dissociation overlaps with other pair distances

and seems to be obscured by them. However, it becomes noticeable at larger pair distances in region γ, where the dissociated CO leads to pair distances that exceed the intramolecular distances of the remaining $Fe(CO)_4$.

We use the simulated pair density dynamics to obtain the simulated scattering signal (Supplementary Discussion 3) and convolved it with the estimated finite instrument response (58 fs, Supplementary Discussion 8). It is then compared to the experimental scattering results in Fig2b. We find that there is reasonable agreement with some minor observed differences that can be attributed to the method used to subtract the experimental background and the limitation of the simulation to capture later dynamics that include the second dissociation (Supplementary Discussions 1,2).

We take the simulated scattering signal and then enforce on it the same constraints as we have for the experiment, and transform it to real space using the method in [35] to obtain the pair density dynamics given the available Q range (Supplementary Discussion 4). In Fig2c, we show the impact of these constraints on the extracted structural dynamics information, highlighting how the spatial resolution of the simulated ΔPD is limited by the experimental Q-range. We observe, that while individual pair distances are not resolved, the underlying dynamics are still recovered. The dominant pair density difference is due to the spectator C-O and O-O pairs at distances of $4<R<6$Å (β region) that capture the onset of synchronous oscillations that originate in the Fe-C pairs. The dissociation is first manifested as an increase of density at these distances at a 200-400 fs delay, following positive contributions to distances >7Å (γ region) at later delays. In addition, we observe a modulation in ΔPD as it evolves from region β to γ. We will discuss these effects and their relation to the rotation of the dissociated CO.

Figure 2d presents the experimental ΔPD following the inversion of the measured scattering difference signal. We observe similar early excited state dynamics at similar pair distances, in agreement with the inversion of the simulated ΔPD. Moreover, the experimental ΔPD allows us to probe longer delays which were not accessible by the simulation. A main characteristic that is noticeable at longer delays ($\tau>400$ fs) is the further depletion of pair density around the α region that coincides with the steady state distance of the Fe-C pairs. The ongoing reduction in pair density within this region can be only attributed to a second CO dissociation and the dynamics of $Fe(CO)_4$ that was formed. Additionally, the rate at which density decreases in region α corresponds to an increase in density between $6.5<R<8$Å for times greater than 700 fs.

When analyzing the measured scattering anisotropy difference for a lower Q range (averaged for $Q<0.9$Å^{-1}) (Fig2b inset), we find that the anisotropy sign and temporal behavior favors the axial direction for the first CO loss (Supplementary Discussion 3), following an anisotropy sign flip at longer delays, indicating that subsequent $Fe(CO)_4$ dynamics and the second dissociation is affected more by equatorial than axial CO ligands (Supplementary Discussion 1). This agrees with the calculation in [16] that predicts that the MLCT transition initiates motion with a preferential loss of axial CO (Supplementary Discussion 3).

In Figure 3, we average the experimental ΔPD across distance regions (α, β, γ) and compare them to the simulated case, up to their termination time (640 fs). The range

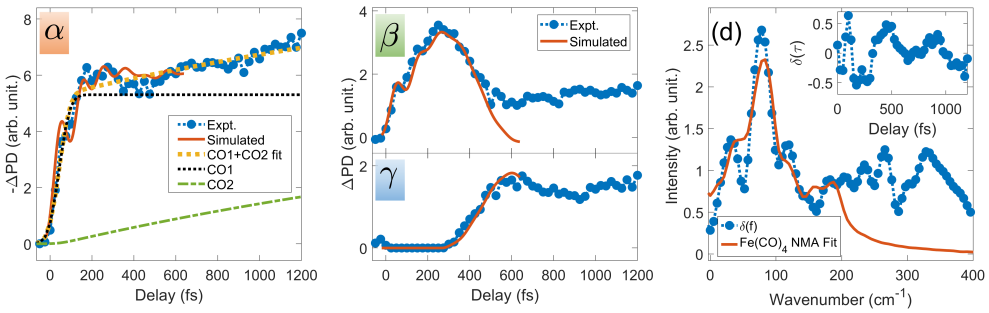

Fig. 3 Observing dissociation and $Fe(CO)_4$ dynamics across various pair distances, compared to simulated (red) pair density dynamics that account only for the first CO loss. (α) Within the range $1.3<R<2.3$Å, steady-state Fe-C pair density tracks CO losses and ground-state Fe-C motions. A kinetic model (dash yellow) fitted to the measured $-\Delta PD$ averaged in this range (blue) yields rates of 94±17 fs (dotted black) and 3±0.5 ps (green) for the first and second dissociation, respectively (see text). (β) Predissociation oscillations are observed at $4<R<7$Å, with the first CO loss marked by a strong peak around 250 fs as Fe-C and Fe-O pairs traverse this distance range. (γ) For $R>7$Å, the first CO loss occurs after 450 fs, followed by the second CO loss visible after 1 ps. (d) Fourier analysis of $\delta(\tau)$, the residual between the fitted CO1+CO2 and measured PD in α (inset) reveals a peak at 78±16 cm^{-1}, attributed to C-Fe-C bending modes in hot $Fe(CO)_4$, as determined by normal mode analysis fit (Supplementary Discussion 7).

in region α provides an opportunity to selectively probe the Fe-C dynamics, being the only pair type in that range. To account for total CO production via dissociation, we consider the averaged $-\Delta PD$ in region α, as every CO leaving the molecule further reduces the Fe-C density of the steady state distances.

The temporal evolution of the experimental ΔPD is then used to fit a kinetic rate model that is based on a previous study [12] and revised to account for the time delay in the onset of dissociation, as detailed in Supplementary Discussion 5. For the first CO dissociation, we obtain a dissociation onset delay of τ_0=43±7 fs due to predissociation oscillatory motion, and a dissociation time constant of τ_1=94±17 fs. For the second dissociation, we obtain a time constant of τ_2=3±0.5 ps, consistent with recent studies [12, 13]. While the predissociation oscillations are less visible in that range, their main signature is better observed in pair distance region β ($4<R<7$Å). In this distance range, the first CO loss is marked by a density peak at 250 fs, coinciding with the Fe-C and Fe-O pairs crossing this range. The simulated ΔPD agrees well with the measured density in all ranges up to the point the second CO loss becomes visible at ∼500 fs. For region γ ($7<R<10$Å), we track the time required for the dissociating pair density to exceed the intramolecular distances of $Fe(CO)_5$. The onset of the second dissociation is marked by a slower density increase beginning at a delay of $\tau > 950fs$. This density growth, with a time constant of 3 ps, is consistent with that observed in region α.

When the experimental ΔPD is subtracted from the kinetic model fit in distance range α, the residual $\delta(\tau)$ reveals distinct oscillations in the 400-1200 fs range (Fig. 3d), with a prominent frequency of 78±16 cm^{-1}. We attribute this motion to C-Fe-C bending modes of the hot $Fe(CO)_4$. This interpretation is supported by a normal mode analysis of the $Fe(CO)_4$ molecule considering various ground state configurations (singlet open shell, singlet closed shell, and triplet). Each normal mode's motion

was translated to its corresponding pair density dynamics using the experimental constraints to determine their relative contributions to the observed frequencies in Fig. 3d. We find that the low-frequency structure (< 100 cm^{-1}) is predominantly (57%) due to singlet closed shell modes at 42 and 79.5 cm^{-1}, with contributions from (30%) singlet open-shell (77.7 and 91.1 cm^{-1}), and (13%) triplet (79.2 and 83.9 cm^{-1}) modes (Supplementary Discussion 7). Our findings are consistent with a recent study that show that both singlet and triplet states are involved in the photodissociation of gas-phase $Fe(CO)_5$ [14].

We further support our findings by referencing earlier studies [36, 37] which identified $Fe(CO)_5$ Raman allowed bending modes at 74.3 and 97.3 cm^{-1}. Contrary to the immediate onset expected from a Raman transition, our observations reveal a delay larger than $\tau_0+\tau_1\approx140$ fs for the measured density oscillations that correspond to the main frequency peak at 78 cm^{-1} (inset of Figure 3d). This delay, which deviates from the instantaneous response expected of a Raman transition induced by single-pulse photoexcitation, suggests that it originates from the formation of $Fe(CO)_4$. Additionally, by excluding earlier times and adjusting the time window for the Fourier transform of $\delta(\tau)$ to start later, we clarify that the broad peak at 330 cm^{-1} arises from predissociation oscillations occurring before 250 fs. This analysis also reveals that the low-frequency structure <200 cm^{-1} emerges from oscillations starting after 400 fs, indicating the main frequency's onset at later times.

In the experimental ΔPD in Figure 2d we observe a density modulation between region β and γ at 300-600 fs, which is also captured in the simulation. This modulation is attributed to the CO rotation as it dissociates, which involves the alternating crossing and separation of dissociative pairs—each consisting of an atom from the remaining $Fe(CO)_4$ and one from the dissociating CO, weighted by their charge product, where the Fe-X pairs dominate the signal.

In Figure 4a, we compare the measured ΔPD modulations with the simulated positions and times at which the dissociative pair distance crossings occur, weighted by their charge density product. We observe agreement between the positions and times of the density modulation and the pair distance crossings. In addition, we observe that the initial enhancement in density in the range β is not only due to the Fe-C pair crossing other intramolecular pairs distances but also due to the CO rotation motion.

The enhancements in ΔPD within regions β and γ, confirmed by simulation, help us estimate the dissociation velocity and rotational frequency of the molecules (Figure 4b), as detailed below. To illustrate the impact of rotation on ΔPD, we examine the Fe-X pair distances from a single trajectory simulation, as shown in Figure 4c. Before dissociation, the Fe-C distance is shorter compared to that between Fe and O. As CO rotates, the distances equalize after a quarter rotation, and with another quarter turn, the Fe-C distance exceeds the Fe-O distance. This alternating crossing and separation of pair distances are captured and result in the modulation of ΔPD as shown in the simulation in Figure 4d.

The dissociation velocity and rotational frequency of CO are quantified using both simulation and experimental results and compared in Fig 4b. From the simulations, we determine the dissociation velocity by averaging over all trajectories the velocity between the dissociating CO center of mass, and the remaining Fe(CO)4 center of

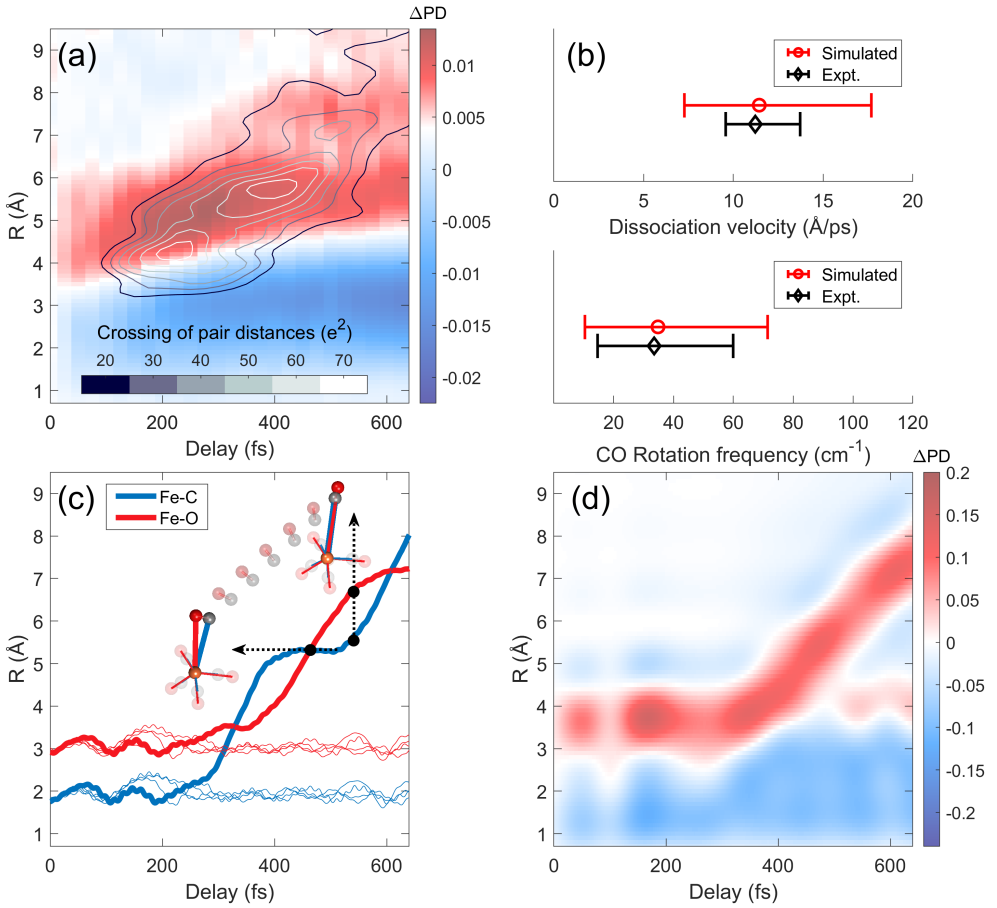

Fig. 4 (a) The measured ΔPD (red-blue) is compared to the simulated density at positions and times where pair distances cross each other (contour), correlating observed density modulations with roto-translational motion. (b) The dissociation velocity and rotation frequency are estimated from the measured ΔPD modulations and compared to the expectation values from the simulation using all trajectories (Supplementary Discussion 6). (c) A single trajectory calculation illustrates the effect of CO dissociation and rotation when pair distances cross each other. Fe-C (blue line) and Fe-O (red line) distances cross (horizontal arrow) and separate (vertical arrow) in space and time as the dissociating CO rotates 90°, which in turn produce the density modulations simulated in (d) using the experimental conditions.

mass, and the rotational CO frequency. The analysis shows a correlation between dissociation velocity and rotation frequency, detailing how energy is divided between translational and rotational motion. We obtain an average dissociation velocity of 11.4 Å/ps and rotational frequency to be 35 cm^{-1} (Supplementary Discussion 6).

Experimentally, the dissociation velocity is estimated by analyzing the onset and progression of dissociation for the Fe-C pair (50-150 fs at 1.85 Å), correlating with the density modulation observed at 400-600 fs and 7-8 Å. The dissociation velocity for CO is thus estimated to be 11.2 $^{+1.7}_{-2.5}$Å/ps. The CO rotational frequency is inferred to

be 34^{+26}_{-19} cm^{-1}, supported by observed modulations that correspond to contributions of 90° and 270° rotation (Supplementary Discussion 6). These results agree with the expectation values that are obtained from the trajectory simulations, and we obtain that the kinetic energy release is partitioned at a 10:1 ratio translational (182 meV) to rotational (17.5 meV). Furthermore, we can assign an upper bound for the dissociation velocity of the second CO loss, using an extended time window post-initial CO loss based on the kinetic model (150-250 fs) at the Fe-C steady state distance, and the appearance of the ΔPD enhancement for $6.5<R<8$ at 700-800 fs. We estimate a dissociation velocity upper bound of $8.5\ ^{+1.2}_{-0.8}$Å$/ps$, and a kinetic energy release of 107 meV (Supplementary Discussion 6).

In conclusion, using UXS and real-space inversion we recover the ultrafast changes in the atomic distances of photoexcited $Fe(CO)_5$. We observed the photoinduced structural oscillations that lead to photodissociation, using the spectator effect, a new approach for observation of atomic motion, captured by the correlated pair density dynamics. This effect can enable tracing motion in complex settings using a deterministic local oscillator to benchmark motion for other pair distances. Moreover, we identify the signature of rotation on the pair density dynamics, recover a correlated rotational motion on the first dissociation process, and characterize its rate and energy release distribution, as well as details of the second thermal dissociation process. A core challenge to understanding chemical reaction mechanisms is determining the nature and duration of deterministic and concerted reaction dynamics prior to the onset of statistical and thermal dynamics. Addressing this challenge requires understanding the dynamics of energy redistribution between the electronic and nuclear degrees of freedom (vibrations, rotations, and translations). By directly accessing all structural degrees of freedom, ultrafast X-ray scattering inverted into real-space and combined with molecular dynamics simulations brings us closer to addressing the challenge of understanding the non-equilibrium flow of energy during chemical reactions.

3 Methods

Ultrafast X-ray scattering: We performed time-resolved gas-phase x-ray scattering experiments at the Coherent x-ray Imaging instrument [38] of the Linac Coherent Light Source (LCLS) at the SLAC National Accelerator Laboratory as previously described [39, 40]. The details regarding Data collection and initial scattering analysis are described in Supplementary Discussion 1. Briefly, $Fe(CO)_5$ (Sigma-Aldrich) was introduced as a room-temperature gas with a pressure of 3 torr and excited by an ultrashort 266-nm pump pulse, and probed by an ultrashort 9.5 keV X-ray pulse. A Cornell-SLAC pixel array detector [41] recorded single-shot scattering patterns, which were binned by their time relative to the pump laser and averaged over multiple shots, with 25 fs time bins, with a randomized sequence of delay steps to avoid systematic errors. The raw detector signal was corrected for the scattering geometry and X-ray polarization, and calibrated using a static scattering signal from sulfur hexafluoride (SF_6) [17]. The time-delayed scattering signal is subtracted from the signal of the unexcited sample, to allow tracing changes in signal positions and cancel background signals $\Delta S(Q,t)=S_{on}(Q,t)-S_{off}(Q)$. We performed pump pulse energy

scans to confirm that we were in the linear absorption regime, and based on the relative signal levels we estimated an excitation fraction of 8% and an instrument response function of 58 fs (Supplementary Discussion 8). From the total scattering signal the isotropic and anisotropic scattering difference curves were obtained $\Delta S(Q,t)=\Delta S_0(Q,t)-P_2(\cos\theta_Q)\Delta S_2(Q,t)$, as detailed in [19], where the signal was detected in the range $0.36<Q<4.34\text{Å}^{-1}$ binned at $\Delta q=0.1208\text{Å}^{-1}$. The isotropic scattering difference signal was inverted following the method described in [35].

Excited state molecular dynamics of $Fe(CO)_5$: The methods for creating the trajectories used in this study were detailed in [16]. SHARC (version 2.1) was employed for ab initio excited state molecular dynamics with surface-hopping, generating an absorption spectrum from 7 singlet states through Wigner distribution of 300 phase space points based on ground state vibrational normal modes. This approach prioritized the S_6 state, aligned with the energy range of the typical UV pulses used in experiments, by limiting the inclusion of higher excited states to prevent deviation to lower wavelength regions. The study in [16] utilized 116 out of 300 Wigner sampled trajectories that successfully transitioned to the S_6 state (indicative of MLCT characteristics). These trajectories, extended to consider 10 singlet states and did not consider triplet states, consistent with the singlet-exclusive pathway for gas phase photodissociation of Fe(CO)5 found in experiment [12]. Out of the 116 trajectories analyzed, 103 were selected for further analysis based on specific criteria. These criteria included the observation of CO dissociation in the trajectories along with suitable termination times averaging 425 fs, which allowed for effective extrapolation. We applied a dissociative atomic rotational-translational model (Supplementary Discussions 2) to extrapolate the prematurely terminated trajectories. This approach enabled us to average the total simulated PD dynamics across all selected trajectories and compare these results with the experimentally measured PD dynamics at the CO dissociation distances at range γ.

Supplementary information. Supplementary Discussions 1–9, Figs. 1–13.

Acknowledgments. This work was supported by the US Department of Energy, Office of Science, Office of Basic Energy Sciences, Chemical Sciences, Geosciences and Biosciences Division. A.S., P.H.B, K.J.G, R.H. K.L. A.K. K.K. J.T.O. R.M.P. A.L.W. M.R.W. T.J.A.W and A.N. were supported by the U.S. Department of Energy, Office of Science, Basic Energy Sciences (BES), Chemical Sciences, Geosciences, and Biosciences Division, AMOS Program. E.B. work was supported by the U.S. Department of Energy, Office of Science, Basic Energy Sciences, Chemical Sciences, Geosciences, and Biosciences Division, Condensed Phase and Interfacial Molecular Science program, FWP 16248. P.M.W. acknowledges funding by the U.S. Department of Energy, Office of Science, Basic Energy Sciences, under award number DE-SC0017995. M.O. acknowledges financial support from the Swedish Research Council (VR contract 2021-04521). The authors gratefully acknowledge support from the Linac Coherent Light Source, SLAC National Accelerator Laboratory, which is supported by the US Department of Energy, Office of Science, Office of Basic Energy Sciences, under contract no. DE-AC02-76SF00515. We acknowledge the help of A.L. Wang-Holtzen and M.R. Ware with the experimental beam-time support.

Conflict of interest/Competing interests. The authors declare no competing interests.

Ethics approval. Not applicable.

Data availability:. The data that support the findings of this study are available from the corresponding author upon reasonable request.

Code availability:. The codes used for the analysis of the raw experimental and simulation data are available from the corresponding authors upon reasonable request.

Authors' contributions:. E.B., S.B., P.H.B., S.C., K.J.G., J.G., R.H., K.L., A.K., J.E.K., K.K., T.J.L., M.L., M.P.M, J.T.O., R.M.P., F.P., S.N., P.M.W., T.J.A.W., A.N. prepared and conducted the experiment at the Linac Coherent Light Source, A.S., E.B., A.N. analysed the experimental data. J.M.R, B.S., M.P.M, P.M.W designed the scattering cell, R.M.P, A.B. M.O. A.N. performed simulations, A.B, M.O performed ab initio calculations. A.N. analyzed and interpreted simulation results, and wrote the article with contributions from all authors.

Appendix A Section title of first appendix

Not applicable

References

[1] Prier, C.K., Rankic, D.A., MacMillan, D.W.C.: Visible light photoredox catalysis with transition metal complexes: Applications in organic synthesis. Chemical Reviews **113**(7), 5322–5363 (2013) https://doi.org/10.1021/cr300503r . PMID: 23509883

[2] Arias-Rotondo, D.M., McCusker, J.K.: The photophysics of photoredox catalysis: a roadmap for catalyst design. Chem. Soc. Rev. **45**, 5803–5820 (2016) https://doi.org/10.1039/C6CS00526H

[3] Wrighton, M.: Photochemistry of metal carbonyls. Chemical Reviews **74**(4), 401–430 (1974) https://doi.org/10.1021/cr60290a001 https://doi.org/10.1021/cr60290a001

[4] Snee, P.T., Payne, C.K., Mebane, S.D., Kotz, K.T., Harris, C.B.: Dynamics of photosubstitution reactions of $Fe(CO)_5$: An ultrafast infrared study of high spin reactivity. Journal of the American Chemical Society **123**(28), 6909–6915 (2001) https://doi.org/10.1021/ja010648r

[5] Wernet, P., Kunnus, K., Josefsson, I., Rajkovic, I., Quevedo, W., Beye, M., Schreck, S., Grübel, S., Scholz, M., Nordlund, D., Zhang, W., Hartsock, R.W., Schlotter, W.F., Turner, J.J., Kennedy, B., Hennies, F., Groot, F.M.F., Gaffney,

K.J., Techert, S., Odelius, M., Föhlisch, A.: Orbital-specific mapping of the ligand exchange dynamics of $Fe(CO)_5$ in solution. Nature **520**(7545), 78–81 (2015) https://doi.org/10.1038/nature14296

[6] Chergui, M.: Ultrafast photophysics of transition metal complexes. Accounts of Chemical Research **48**(3), 801–808 (2015) https://doi.org/10.1021/ar500358q . PMID: 25646968

[7] Chen, L.X., Zhang, X., Shelby, M.: Recent advances on ultrafast x-ray spectroscopy in the chemical sciences. Chemical science **5**(11), 4136–4152 (2014)

[8] Poliakoff, M., Weitz, E.: Shedding light on organometallic reactions: the characterization of tetracarbonyliron ($Fe(CO)_4$), a prototypical reaction intermediate. Accounts of Chemical Research **20**(11), 408–414 (1987) https://doi.org/10.1021/ar00143a004

[9] Trushin, S., Fuss, W., Kompa, K., Schmid, W.: Femtosecond dynamics of $Fe(CO)_5$ photodissociation at 267 nm studied by transient ionization. The Journal of Physical Chemistry A **104**(10), 1997–2006 (2000)

[10] Fuss, W., Trushin, S., Schmid, W.: Ultrafast photochemistry of metal carbonyls. Research on Chemical Intermediates **27**(4), 447–457 (2001)

[11] Trushin, S.A., Fuß, W., Schmid, W.E.: Dissociative ionization at high laser intensities: Importance of resonances and relaxation for fragmentation. Journal of Physics B: Atomic, Molecular and Optical Physics **37**(19), 3987 (2004)

[12] Wernet, P., Leitner, T., Josefsson, I., Mazza, T., Miedema, P.S., Schröder, H., Beye, M., Kunnus, K., Schreck, S., Radcliffe, P., Düsterer, S., Meyer, M., Odelius, M., Föhlisch, A.: Communication: Direct evidence for sequential dissociation of gas-phase $Fe(CO)_5$ via a singlet pathway upon excitation at 266 nm. The Journal of Chemical Physics **146**(21), 211103 (2017) https://doi.org/10.1063/1.4984774 https://pubs.aip.org/aip/jcp/article-pdf/doi/10.1063/1.4984774/13595045/211103_1_online.pdf

[13] Cole-Filipiak, N.C., Troß, J., Schrader, P., McCaslin, L.M., Ramasesha, K.: Ultraviolet photodissociation of gas-phase iron pentacarbonyl probed with ultrafast infrared spectroscopy. The Journal of Chemical Physics **154**(13), 134308 (2021) https://doi.org/10.1063/5.0041074 https://pubs.aip.org/aip/jcp/article-pdf/doi/10.1063/5.0041074/15588793/134308_1_online.pdf

[14] Troß, J., Arias-Martinez, J.E., Carter-Fenk, K., Cole-Filipiak, N.C., Schrader, P., McCaslin, L.M., Head-Gordon, M., Ramasesha, K.: Femtosecond core-level spectroscopy reveals involvement of triplet states in the gas-phase photodissociation of fe(co)5. Journal of the American Chemical Society **146**(32), 22711–22723 (2024) https://doi.org/10.1021/jacs.4c07523 https://doi.org/10.1021/jacs.4c07523. PMID: 39092878

[15] Ihee, H., Cao, J., Zewail, A.H.: Ultrafast electron diffraction of transient [$Fe(CO)_4$]: Determination of molecular structure and reaction pathway. Angewandte Chemie International Edition **40**(8), 1532–1536 (2001)

[16] Banerjee, A., Coates, M.R., Kowalewski, M., Wikmark, H., Jay, R.M., Wernet, P., Odelius, M.: Photoinduced bond oscillations in ironpentacarbonyl give delayed synchronous bursts of carbonmonoxide release. Nature Communications **13**(1), 1337 (2022)

[17] Glownia, J.M., Natan, A., Cryan, J.P., Hartsock, R., Kozina, M., Minitti, M.P., Nelson, S., Robinson, J., Sato, T., Driel, T., Welch, G., Weninger, C., Zhu, D., Bucksbaum, P.H.: Self-referenced coherent diffraction x-ray movie of ångstrom- and femtosecond-scale atomic motion. Phys. Rev. Lett. **117**, 153003 (2016) https://doi.org/10.1103/PhysRevLett.117.153003

[18] Bucksbaum, P.H., Ware, M.R., Natan, A., Cryan, J.P., Glownia, J.M.: Characterizing multiphoton excitation using time-resolved x-ray scattering. Phys. Rev. X **10**, 011065 (2020) https://doi.org/10.1103/PhysRevX.10.011065

[19] Natan, A., Schori, A., Owolabi, G., Cryan, J.P., Glownia, J.M., Bucksbaum, P.H.: Resolving multiphoton processes with high-order anisotropy ultrafast x-ray scattering. Faraday Discussions **228**, 123–138 (2021)

[20] Kierspel, T., Morgan, A., Wiese, J., Mullins, T., Aquila, A., Barty, A., Bean, R., Boll, R., Boutet, S., Bucksbaum, P., *et al.*: X-ray diffractive imaging of controlled gas-phase molecules: Toward imaging of dynamics in the molecular frame. The Journal of Chemical Physics **152**(8), 084307 (2020)

[21] Wolf, T.J., Sanchez, D.M., Yang, J., Parrish, R., Nunes, J., Centurion, M., Coffee, R., Cryan, J., Gühr, M., Hegazy, K., *et al.*: The photochemical ring-opening of 1, 3-cyclohexadiene imaged by ultrafast electron diffraction. Nature chemistry **11**(6), 504–509 (2019)

[22] Champenois, E., Sanchez, D., Yang, J., Figueira Nunes, J., Attar, A., Centurion, M., Forbes, R., Gühr, M., Hegazy, K., Ji, F., *et al.*: Conformer-specific photochemistry imaged in real space and time. Science **374**(6564), 178–182 (2021)

[23] Yang, J., Zhu, X., F. Nunes, J.P., Yu, J.K., Parrish, R.M., Wolf, T.J., Centurion, M., Gühr, M., Li, R., Liu, Y., *et al.*: Simultaneous observation of nuclear and electronic dynamics by ultrafast electron diffraction. Science **368**(6493), 885–889 (2020)

[24] Ihee, H., Wulff, M., Kim, J., Adachi, S.-i.: Ultrafast x-ray scattering: structural dynamics from diatomic to protein molecules. International Reviews in Physical Chemistry **29**(3), 453–520 (2010)

[25] Kim, K.H., Kim, J.G., Nozawa, S., Sato, T., Oang, K.Y., Kim, T.W., Ki, H., Jo, J., Park, S., Song, C., *et al.*: Direct observation of bond formation in solution with femtosecond x-ray scattering. Nature **518**(7539), 385–389 (2015)

[26] Biasin, E., Driel, T.B., Kjær, K.S., Dohn, A.O., Christensen, M., Harlang, T., Vester, P., Chabera, P., Liu, Y., Uhlig, J., Pápai, M., Németh, Z., Hartsock, R., Liang, W., Zhang, J., Alonso-Mori, R., Chollet, M., Glownia, J.M., Nelson, S., Sokaras, D., Assefa, T.A., Britz, A., Galler, A., Gawelda, W., Bressler, C., Gaffney, K.J., Lemke, H.T., Møller, K.B., Nielsen, M.M., Sundström, V., Vankó, G., Wärnmark, K., Canton, S.E., Haldrup, K.: Femtosecond x-ray scattering study of ultrafast photoinduced structural dynamics in solvated $[Co(terpy)_2]^{2+}$. Phys. Rev. Lett. **117**, 013002 (2016) https://doi.org/10.1103/PhysRevLett.117.013002

[27] Chollet, M., Alonso-Mori, R., Cammarata, M., Damiani, D., Defever, J., Delor, J.T., Feng, Y., Glownia, J.M., Langton, J.B., Nelson, S., al.: The x-ray pump–probe instrument at the linac coherent light source. Journal of Synchrotron Radiation **22**(3), 503–507 (2015) https://doi.org/10.1107/S1600577515005135

[28] Van Driel, T.B., Kjær, K.S., Hartsock, R.W., Dohn, A.O., Harlang, T., Chollet, M., Christensen, M., Gawelda, W., Henriksen, N.E., Kim, J.G., *et al.*: Atomistic characterization of the active-site solvation dynamics of a model photocatalyst. Nature communications **7**(1), 1–7 (2016)

[29] Haldrup, K., Levi, G., Biasin, E., Vester, P., Laursen, M.G., Beyer, F., Kjær, K.S., Driel, T., Harlang, T., Dohn, A.O., Hartsock, R.J., Nelson, S., Glownia, J.M., Lemke, H.T., Christensen, M., Gaffney, K.J., Henriksen, N.E., Møller, K.B., Nielsen, M.M.: Ultrafast x-ray scattering measurements of coherent structural dynamics on the ground-state potential energy surface of a diplatinum molecule. Phys. Rev. Lett. **122**, 063001 (2019) https://doi.org/10.1103/PhysRevLett.122.063001

[30] Gabalski, I., Sere, M., Acheson, K., Allum, F., Boutet, S., Dixit, G., Forbes, R., Glownia, J.M., Goff, N., Hegazy, K., Howard, A.J., Liang, M., Minitti, M.P., Minns, R.S., Natan, A., Peard, N., Rasmus, W.O., Sension, R.J., Ware, M.R., Weber, P.M., Werby, N., Wolf, T.J.A., Kirrander, A., Bucksbaum, P.H.: Transient vibration and product formation of photoexcited CS2 measured by time-resolved x-ray scattering. The Journal of Chemical Physics **157**(16), 164305 (2022) https://doi.org/10.1063/5.0113079 https://pubs.aip.org/aip/jcp/article-pdf/doi/10.1063/5.0113079/16553691/164305_1_online.pdf

[31] Powers-Riggs, N.E., Birgisson, B.O., Raj, S.L., Biasin, E., Lenzen, P., Zederkof, D.B., Haubro, M., Tveiten, D.K.V., Hartsock, R.W., Driel, T.B., Kunnus, K., Chollet, M., Robinson, J.S., Nelson, S., Forbes, R., Haldrup, K., Pedersen, K.S., Levi, G., Ougaard Dohn, A., Jónsson, H., Møller, K.B., Natan, A., Nielsen, M.M., Gaffney, K.J.: Characterization of deformational isomerization potential

and interconversion dynamics with ultrafast x-ray solution scattering. Journal of the American Chemical Society **146**(20), 13962–13973 (2024) https://doi.org/10.1021/jacs.4c00817 https://doi.org/10.1021/jacs.4c00817. PMID: 38727611

[32] Minitti, M.P., Budarz, J.M., Kirrander, A., Robinson, J.S., Ratner, D., Lane, T.J., Zhu, D., Glownia, J.M., Kozina, M., Lemke, H.T., Sikorski, M., Feng, Y., Nelson, S., Saita, K., Stankus, B., Northey, T., Hastings, J.B., Weber, P.M.: Imaging molecular motion: Femtosecond x-ray scattering of an electrocyclic chemical reaction. Phys. Rev. Lett. **114**, 255501 (2015) https://doi.org/10.1103/PhysRevLett.114.255501

[33] Ruddock, J.M., Zotev, N., Stankus, B., Yong, H., Bellshaw, D., Boutet, S., Lane, T.J., Liang, M., Carbajo, S., Du, W., *et al.*: Simplicity beneath complexity: counting molecular electrons reveals transients and kinetics of photodissociation reactions. Angewandte Chemie **131**(19), 6437–6441 (2019)

[34] Ruddock, J.M., Yong, H., Stankus, B., Du, W., Goff, N., Chang, Y., Odate, A., Carrascosa, A.M., Bellshaw, D., Zotev, N., Liang, M., Carbajo, S., Koglin, J., Robinson, J.S., Boutet, S., Kirrander, A., Minitti, M.P., Weber, P.M.: A deep uv trigger for ground-state ring-opening dynamics of 1,3-cyclohexadiene. Science Advances **5**(9), 6625 (2019) https://doi.org/10.1126/sciadv.aax6625 https://www.science.org/doi/pdf/10.1126/sciadv.aax6625

[35] Natan, A.: Real-space inversion and super-resolution of ultrafast scattering. Phys. Rev. A **107**, 023105 (2023) https://doi.org/10.1103/PhysRevA.107.023105

[36] Bigorgne, M.: Étude spectroscopique raman et infrarouge de$Fe(CO)_5$, fe (co) 4l et trans-fe (co) 3l2 (l= pme3, asme3, sbme3) i. attribution des bandes de$Fe(CO)_5$. Journal of Organometallic Chemistry **24**(1), 211–229 (1970)

[37] Jones, L.H., McDowell, R.S., Goldblatt, M., Swanson, B.I.: Potential constants of iron pentacarbonyl from vibrational spectra of isotopic species. The Journal of Chemical Physics **57**(5), 2050–2064 (1972)

[38] Liang, M., Williams, G.J., Messerschmidt, M., Seibert, M.M., Montanez, P.A., Hayes, M., Milathianaki, D., Aquila, A., Hunter, M.S., Koglin, J.E., Schafer, D.W., Guillet, S., Busse, A., Bergan, R., Olson, W., Fox, K., Stewart, N., Curtis, R., Miahnahri, A.A., Boutet, S.: The Coherent X-ray Imaging instrument at the Linac Coherent Light Source. Journal of Synchrotron Radiation **22**(3), 514–519 (2015) https://doi.org/10.1107/S160057751500449X

[39] Budarz, J.M., Minitti, M.P., Cofer-Shabica, D.V., Stankus, B., Kirrander, A., Hastings, J.B., Weber, P.M.: Observation of femtosecond molecular dynamics via pump–probe gas phase x-ray scattering. Journal of Physics B: Atomic, Molecular and Optical Physics **49**(3), 34001 (2016) https://doi.org/10.1088/0953-4075/49/3/034001

[40] Stankus, B., Yong, H., Zotev, N., Ruddock, J.M., Bellshaw, D., Lane, T.J., Liang, M., Boutet, S., Carbajo, S., Robinson, J.S., *et al.*: Ultrafast x-ray scattering reveals vibrational coherence following rydberg excitation. Nature chemistry **11**(8), 716–721 (2019)

[41] Hart, P., Boutet, S., Carini, G., Dubrovin, M., Duda, B., Fritz, D., Haller, G., Herbst, R., Herrmann, S., Kenney, C., *et al.*: The cspad megapixel x-ray camera at lcls. In: X-Ray Free-electron Lasers: Beam Diagnostics, Beamline Instrumentation, and Applications, vol. 8504, p. 85040 (2012). International Society for Optics and Photonics